# Mobile Energy Storage Scheduling and Operation in Active Distribution Systems

Hussein Hassan Abdeltawab, and Yasser Abdel-Rady I. Mohamed, *Senior Member*, *IEEE*

***Abstract*—A mobile (transportable) energy storage system (MESS) can provide various services in distribution systems including load leveling, peak shaving, reactive power support, renewable energy integration and transmission deferral. Unlike stationary energy storage units, a mobile energy storage system can move between different buses by a truck to provide different local services within the distribution feeder. This work proposes a day-ahead energy management system (EMS) for a MESS that aims to minimize the cost of the power imported from the grid. The MESS does not only shift renewable energy power to load peak-hours but also can provide localized reactive power support. Given the day-ahead predictions, the EMS decided the optimal MESS stations in the feeder and the operating power. Next, a particle swarm optimization-based algorithm is developed to tune the moving time of the MESS according to a transit delay model. The applicability of the proposed scheduling and operation algorithms is tested on a typical 41-bus radial feeder.**

***Index Terms*—Day-ahead market, energy management system, mobile energy storage system, model predictive control, transportable energy storage.**

## Nomenclature

### Acronyms

| | |
|---|---|
| DG | Distributed Generation |
| EMS | Energy Management system |
| MESS | Mobile Energy Storage System |
| SESS | Stationary Energy Storage System |
| PSO | Particle Swarm Optimization |
| RES | Renewable Energy Source |
| MPC | Model Predictive Control |
| DNO | Distribution Network Operator |
| EV | Electric Vehicle |
| ESS | Energy Storage System |
| FIT | Fixed Feed-in tariff |
| PSO | Particle Swarm Optimization |

### Sets, indices

| | |
|---|---|
| $\mathcal{N}_s$ | Set of MESS stations |
| $\mathcal{N}_b$ | Set of all system buses |
| $\mathcal{N}_t$ | Set of all system branches |
| $\mathcal{N}_k$ | Set of prediction horizon or time |
| $\mathcal{N}_l$ | Set of load at each bus |
| $\mathcal{N}_r$ | Set of RES at each bus |
| $\mathcal{N}_g$ | Set of DGs at each bus |
| $\mathcal{N}_\tau$ | Set of transit time samples |
| $j$ | Index for MESS destination station |
| $i$ | Index for MESS current station |
| $k$ | Index for time |
| $b$ | Index for bus |
| $s$ | Index for MESS station bus location |
| $g$ | Index for DG bus location |
| $l$ | Index for load bus location |
| $r$ | Index for RES bus location |
| $t, h$ | Index for branch connecting two buses a and b |
| $a$ | Index for start bus of branch t |
| $b$ | Index for end bus of branch t |
| $n$ | Index for a particle of population in PSO |
| $\alpha$ | Index for PSO iteration time |

### Parameters

| | |
|---|---|
| $\eta_{ch}, \eta_{dh}$ | Charge and Discharge efficiency |
| $\mathcal{S}$ | The number of MESS stations |
| $d_{ij}$ | Distance between two MESS stations I, j |
| $Dist$ | Distance matrix between MESS stations |
| $tc_{ijk}$ | The traffic congestion delay if MESS is moving station i into j at time k |
| $\tau_{ijk}$ | the traffic delay if MESS is moving station i into j at time k |
| $V_{avg}$ | the average truck speed |
| $t_{ins}$ | The MESS installation time |
| $T_s$ | The sample time in minutes. |
| $\mathcal{K}$ | Prediction horizon samples size |
| $N_{trips}$ | Maximum number of daily trips |
| $q_{lk}$ | load l reactive power at time k |
| $p_{lk}$ | load l active power at time k |
| $q_{gk}$ | Generator g reactive power at time k |
| $p_{gk}$ | Generator g active power at time k |
| $q_{rk}$ | Renewable source r reactive power at time k |
| $p_{rk}$ | Renewable source r active power at time k |
| $\bar{\ell}_t$ | Branch t ampacity |
| $\underline{v}$ | Minimum permissible voltage level in PU |
| $\overline{v}$ | Maximum permissible voltage level in PU |
| $\bar{E}_s$ | MESS rated energy in kWh |
| $\bar{p}_s$ | MESS rated power in kW |
| $\bar{s}$ | MESS converter rated apparent power in kVA |
| $\underline{SOC}$ | Minimum state of charge in PU |
| $\overline{N}$ | Maximum number of cycle in PU |
| $\Re$ | Number of RES in the system |
| $\mathcal{g}$ | Number of DGs in the system |
| $C_{DG}$ | DG power generation cost |
| $C_{res}$ | RES power generation cost |
| $C_{truck}$ | MESS daily truck running cost |
| $FC$ | Truck fuel consumption cost |
| $tlc$ | Truck labor daily cost |
| $BP_k$ | Energy buy price at time k |
| $C_{kwh}$ | Energy storage levelised cost per kWh |
| $SP_k$ | Energy sell price at time k |
| $inc$ | Income to the DNO |
| $M$ | Transit time limit in PSO |
| $n$ | population-size in PSO |
| $C_1$, $C_2$ | Local and global best position constants in PSO |
| $\bar{\alpha}$ | Maximum number of iterations in PSO |

### Decision Variables

| | |
|---|---|
| $I_{srefk}$ | Storage current controller set point at time k |

Manuscript received January 21, 2016; revised April 08, 2016 and May 27, 2016; accepted July 19, 2016.

The authors are with the Department of Electrical and Computer Engineering, University of Alberta, Edmonton, AB, T6G2V4 Canada (email: abdeltaw@ualberta.ca, yasser_rady@ieee.org).

| | |
|---|---|
| $q_{sk}$ | Storage s reactive power at time k |
| $p_{sk}$ | Storage s active power at time k |
| $q_{bk}$ | Bus b reactive power at time k |
| $p_{bk}$ | Bus b active power at time k |
| $\mathcal{p}_{tk}$ | Branch t active power at time k |
| $q_{tk}$ | Branch t reactive power at time k |
| $\ell_{tk}$ | Branch t second norm current at time k |
| $v_{bk}$ | Bus b second norm voltage at time k |
| $I_{tk}$ | Branch t current at time k |
| $V_{bk}$ | Bus b voltage at time k |
| $z_{sk}$ | MESS existence flag at station s at time k. |
| $y_k$ | MESS is in transit at time k |
| $loss_k$ | System power losses at time k |
| $p_{ch_{sk}}$ | MESS charge power at time k for station s |
| $p_{dh_{sk}}$ | MESS discharge power at time k for station s |
| $SOC_k$ | MESS state of charge at time k |
| $N_{k+1}$ | MESS number of cycles at time k |
| $C_{mess}$ | MESS total running cost |
| $C_{ess}$ | MESS energy storage cost |
| $C_{grid}$ | Grid exported energy cost |
| $P_{gridk}$ | Grid energy at time k |
| $pro$ | profit to the DNO |
| $\mathcal{R}pro$ | Real profit after considering the transit delay effect |
| $\mathcal{R}SOC$ | Real SOC after considering the transit delay effect |
| $\mathcal{R}N$ | Real number of cycles after considering the transit delay effect |
| $Pbest$ | Local best particle location in PSO |
| $Gbest$ | Global best particle location in PSO |
| $\omega(\alpha)$ | Particles inertia at iteration $\alpha$ in PSO |
| $V^n(\alpha)$ | Particle n speed at iteration $\alpha$ |
| $x^n(\alpha)$ | Particle n location during iteration $\alpha$ |

## I. Introduction

TOMORROW's distribution system will witness an increasing penetration level of renewable energy resources (RESs). Because RESs are not dispatchable, the distribution network operator (DNO) faces system security and power quality problems [1]. The DNO can add energy a stationary storage systems (SESSs) to compensate for the intermittent nature of RESs and improve his profitability as well. SESSs have many other power applications including load shifting, energy arbitrage and peak shaving [2], [3]. Besides, SESSs can participate in ancillary services markets to provide online or offline reserve [4]. Also, SESSs can improve the voltage quality by supplying the grid reactively (e.g., in long radial distribution feeder) [5]. Indeed, energy storage provides various energy and ancillary services to the grid which requires developing different EMS strategies both on the device level [6] or and the system level [7], [8]. Different EMS strategies optimize different economic cost functions (maximizing profit, minimizing energy cost or power losses) and limited by system-dependent operational constraints (voltage level, battery energy and power ratings) as in [9], [10] and [11]. Further, the current development in EV industry [7], [12] has boosted the interest of developing smarter EMS techniques.

Like SESS, mobile storage such as electric vehicles (EVs) provide various services to the grid as well. For example, although demand response has the ability of providing energy cost reduction (via load shifting to the off peak hours) [13], combining EVs with demand response has proven to improve the power balance and demand response management results [14]. Using EVs is an effective solution for renewable sources intermittency problem in microgrids [15]. Besides, when EVs are controlled to regulate PV power intermittency, it leads to a significant cost minimization in PV-powered charging stations [16]. Aggregated EVs in parking lots can participate in vehicle to grid (V2G) and grid to vehicle (G2V) programs to reduce energy cost via energy arbitrage [17] and/or participating in the reserve market [18].

Unlike EVs, MESS is a utility-scale storage bank (e.g., lithium-ion battery) owned and fully controlled by the utility company. The storage is mobilized by a big truck and connected to the system at different stations. The advantage of transportability is the ability to deliver a localized reactive power support, power losses reduction, voltage regulation, dispersed RESs integration, and T&D upgrade deferral. MESS is available commercially in 100, 1000 and 5000 kW ratings [19]. An example for a MESS prototype project is a 500 kW/1000 kWh project for tea industry peak shaving in China [20]. MESS has been investigated by research centers such as the Electric Power Research Institute (EPRI) [21], [22]. Another project under investigation is a 500 kW/776 kWh SCiBTM lithium-ion battery for peak shaving and voltage regulation in a distribution system. The project is located in Spain and conducted by Toshiba Cooperation [23]. Further advantages for MESS are mentioned in the research motivation explained in Section II.

The MESS is a promising storage technology that will contribute to solve many issues in active distribution systems. Optimal scheduling and energy management algorithms for a MESS in an active distribution system are not developed in the current literature. This work proposes a day-ahead energy management system (EMS) for a MESS owned by a DNO. The DNO uses the MESS for minimizing the day-ahead cost of power imported from the grid. Further, MESS provides a reactive power support for the system for voltage regulation at critical loads. The authors want to emphasize that this work does not compare by any mean the fixed ESS with the Mobile one from the economic point of view, rather this work presents a management system if the DNO found a MESS investment is a profitable one. The main contributions of this work to the research field are as follows:

1. Developing an EMS system for a MESS that 1) dispatches the MESS, and 2) schedules the truck positions.
2. Developing a MESS transition delay model.
3. Converting the nonconvex optimization problem into a convex one via the proposed two-stage technique.

This rest of the paper is organized as follows. Firstly, the system description is presented in Section II. Section III presents the proposed EMS and scheduling framework for the MESS. Simulation results are presented in Section IV. Finally, the conclusions are drawn in Section V.

## II. Problem Description

### A. Motivation

Still with the increasing number of RESs dispersed in the system, a large number of ESSs is needed to support the grid stability and reliability. This results in an infeasible investment from the economic point of view for two main reasons. First, the high cost of ESSs and its relatively low lifetime. Second, the ESS cost diminishes with its rating, thus, a large number of ESSs has way much cost than a single unit with the same capacity. According to [24], the ESS power conversion system

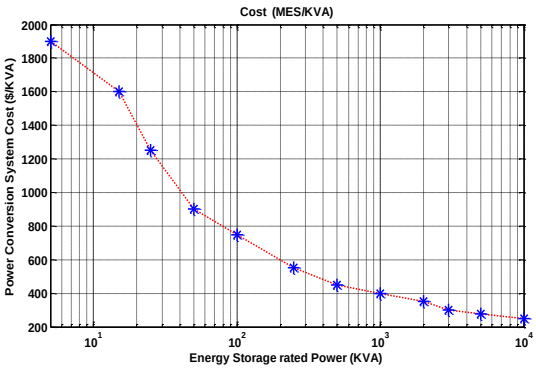


Fig. 1. Power conversion system cost verses size.

per-unit cost varies from (1,800$/kW) for a 5 kW station to (300$/kW) for a 2 MW one as shown in Fig. 1. As a result, a significant saving is achievable if a single bulk ESS can replace a large number of smaller ESSs. However, distributed ESSs provide some localized services that a single centralized ESS cannot provide such as voltage regulation or power losses minimization. An MESS solves this problem because an MESS is a single ESS that can be plugged into the system at different locations during different times, it can provide different localized grid services in a way much cheaper than multi stationary ESSs (SESSs). The advantage of transportability is the ability to deliver a localized reactive power support for voltage regulation, power losses reduction, dispersed RESs integration, and last but not least, transmission and distribution upgrade deferral.

Indeed, aggregated EVs looks like a cheaper similar solution for providing grid services exactly like the MESS. A similar solution where the network operator does not have to invest any initial cost, however; aggregated EVs in parking lot has both power and energy uncertainty due to its uncontrollable availability time [17] which question the reliability of the service. Besides, it requires a high number of EVs to give the same power rating equivalent to a single MESS truck. Besides, not all the EVs owners are willing to participate in grid services [16].

This article does not claim by any mean that MESS will always prove to be financially attractive than aggregated EVs or SESSs. Rather, a feasibility study that compares all the different technologies should be conducted for a given system to select the best option from the technical and economic perspectives.

### B. MESS Model

Fig. 2 shows an example of a radial feeder. The feeder has RESs set $\mathcal{N}_r$ at different locations of the feeder, such as wind energy conversion systems (WECS) and photovoltaic (PV) power generators. Furthermore, other dispatchable resources (such as microturbines) exist at different buses and defined by the set $\mathcal{N}_g$. Moreover, the feeder has a load set $\mathcal{N}_l$ with some smart houses (net-zero houses) that may use a rooftop PV, heat pumps, electric storage, and electric vehicle. RESs have different profiles that can be forecasted efficiently using both numerical and physical techniques (e.g., [25]). Moreover, electrical loads can be accurately predicted for the day-ahead operation planning [26], [27]. It should be emphasized that even with a 10-15% power prediction error, a day-ahead EMS

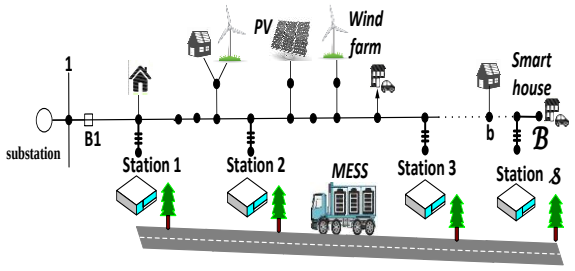


Fig. 2. Radial feeder with multi-MESS stations.

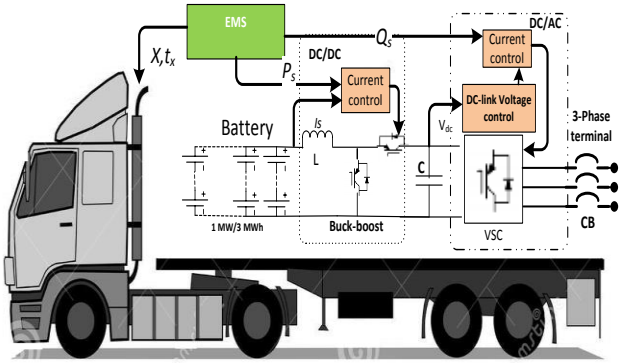


Fig. 3. Mobile energy storage system description.

cannot reach an optimal solution; rather, a day-ahead EMS provides a sub-optimal solution. In order to compensate for the forecast error, a real-time controller is required to adjust the EMS solution depending on actual system measurements. For instance, a day-ahead EMS decides the reactive power set-point; however, due to unpredictable real-time changes (sudden load change, faults or outages, RES intermittency), the actual reactive power is tuned by a real-time on-line voltage controller that measures the bus voltage and tunes the reactive power accordingly. This multi-level control scheme has been adopted widely in the literature such as in [28]. In power system dispatch, the system operator adopts the same strategy when it comes to frequency control. The operator measures the frequency deviation and the power imbalance to decide the area control error (ACE), then the operator starts adjusting its day-ahead schedule by dispatching its reserve resources in real-time accordingly to compensate the ACE [29].

The DNO can schedule a MESS to move between different positions for multi-services. Different MESS positions ($\mathcal{N}_s = \{1,2,..,8\}$) define the buses at which the MESS can be connected to the system which will be designated as the *MESS-stations*. Fig. 3 depicts the structure of a MESS which consists of two parts: the ESS and the truck. The ESS consists of an array of battery cells (e.g., lithium-ion).

While the battery bank terminal voltage is determined by the number of series cells in the same string, the total current is the sum of the parallel strings currents. The reader is referred to IEEE standards 485 [30] for further sizing details. The ESS is connected to the grid via a DC/DC/AC bidirectional VSC. The DC/DC converter is a current-controlled buck-boost controller. The current controller regulates the charging (discharging) power according to the set point provided by the EMS. When the EMS sends the active power set point at time $k$ ($P_{sk}$) to

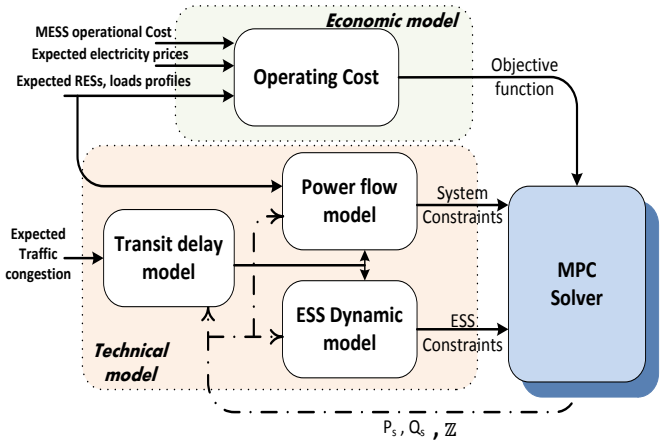


Fig. 4. System techno-economic model structure.

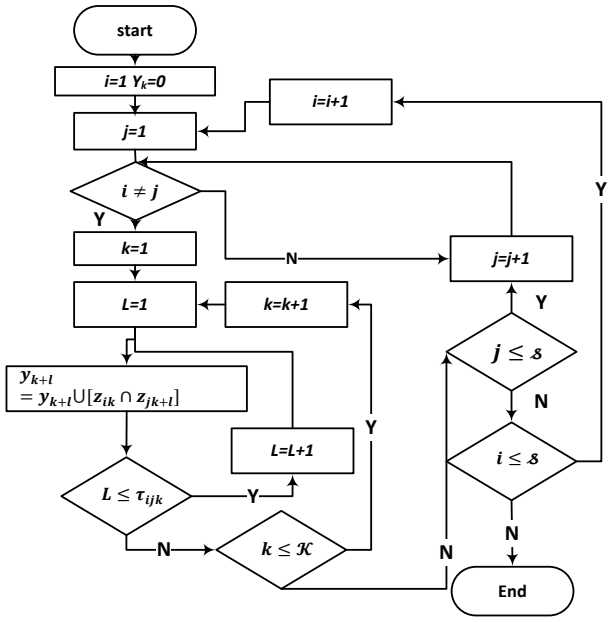


Fig. 5. Transit delay model generation.

the DC/DC current controller, the controller calculates the current set point $I_{sref}$ by dividing the power on the battery bank voltage ($V_{sk}$); $I_{srefk} = \frac{p_{sk}}{V_{sk}}$.The current controller is a proportional-integral (PI) controller that regulates the battery current by manipulating the modulation index of the buck-boost converter [31]. On the other hand, the DC/AC converter transfers the power to (from) the grid via regulating the dc-link voltage [31]. In the *dq*-frame, the dc-link voltage controller decides the VSC-direct current set point whereas the EMS controls the reactive power $q_{sk}$ via changing the quadrature current set point. Further details on the design of the current and dc-link voltage controllers can be found in [31]. A fast charging module is also available in some commercial versions [19].The truck path is also controlled via the EMS. The driver requires a schedule for the MESS- stations that include the station number $\mathcal{s}$ and the transition time to this station $t_s$. To sum up, the DNO needs to design an EMS system for a MESS that generates two set of outputs.

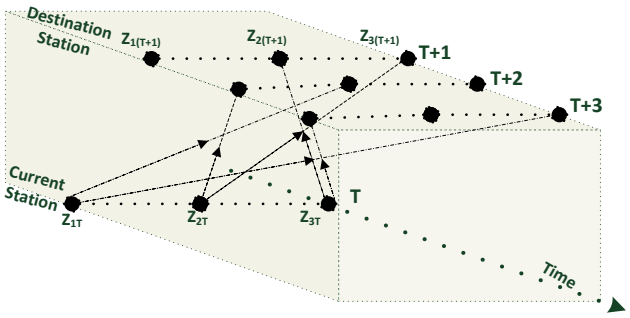


Fig. 6 Transition scenarios example for a three MESS station at sample *k*.

First, the EMS calculates the ESS active and reactive power at each sample. Second, the EMS defines the desired station at each time and the transition time to this station. Next, the EMS design is explained in details.

## III. Energy Management System

To design the EMS for a MESS, a complete techno-economic model, as depicted in Fig. 4, is required. The technical model is composed of three subsystems: 1) the transit delay model that describes the commute time between two stations; 2) the power flow model that relates (the buses voltage, line current and power losses) to the MESS power and positions; and 3) the ESS dynamic model that represents the battery dynamics. The economic model defines different costs of all resources that are reflected in the EMS objective function.

### A. *Transit Delay Model*

The delay model depends on both time and stations positions. For a set of stations $\mathcal{N}_s$, the distance between stations is defined by the distance matrix $Dist$ with a zero diagonal, any element $d_{ij} \forall i,j \in \mathcal{N}_s$ define the distance between stations $(i,j)$. In case $d_{ij} = d_{ji}$, then the MESS uses the same road between two stations $(i,j)$.

$$Dist = \begin{bmatrix} 0 & \cdots & d_{1\mathcal{s}} \\ \vdots & \ddots & \vdots \\ d_{\mathcal{s}1} & \cdots & 0 \end{bmatrix} \quad (1)$$

The traffic congestion delay $tc_{ijk}$ is a time and location dependent index can give an indicator [32] for the traffic delay. $\tau_{ijk}$is the commute time (in samples) from a station *i* to *j* at time $k \in \mathcal{N}_k$which is composed from three parts: the commute time, traffic congestion delay and installation time

$$\tau_{ijk} = round\left(\frac{tc_{ijk} + d_{ij}V_{avg} + t_{ins}}{T_s}\right) \forall i,j \in \mathcal{N}_s, k \in \mathcal{N}_k, i \neq j \quad (2)$$

In (2), $V_{avg}$ is the average truck speed, $t_{ins}$ is the MESS installation time (the connection of MESS to the grid at the station). $T_s$ is the sample time in minutes. For the sake of the modeling, let us define the Boolean matrix $\mathbb{z} \in \mathcal{R}^{\mathcal{s}\times\mathcal{K}}$, where each element $z_{ik}$ equals one if the MESS exists at station *i* at sample time *k*. Next, let us define the Boolean vector $\mathbb{Y} \in \mathcal{R}^{\mathcal{K}}$ that represents the delay model. If the MESS is in transit at a sample *T* due to moving from a station *i* to reach another one *j* after an $\tau_{ijT}$ samples of transition delay*:* $z_{iT} = z_{jT+\tau_{ijT}} = 1, i \neq j \; \forall i,j \in \mathcal{N}_s$. Then $y_{k+l} = 1, l \in [1, \tau_{ijT}], k = T$ In order to define $y_k$, all previous transit conditions that will lead to a future transit delay are modelled. By this way, $y_k$ is expressed

as a sum of minimum terms that represent all possible previous transits as shown in Fig. 5. An example for defining $y_k$ for three stations is depicted in Fig. 6. In this example, three MESS stations exist; thus at any transit instant $T$, the nonzero transitions depend on the current MESS station and the next MESS destination with the following transition delay $\tau_{12T} = 1\ \tau_{23T} = 2\ \tau_{13T} = 3\ \tau_{ijT} = \tau_{jiT}$. As shown in Fig. 6, there are six possible transition scenarios at this sample time (2 possible transitions from each current station). Any transition scenario occurs if both the current and destination stations equal one ($z_{ik} = z_{jk+l} = 1 \rightarrow z_{ik} \cap z_{jk+l} = z_{ik+1}z_{jk} = 1$). Finally, the aggregation of all possible transitions for a certain transit time $T$ is defined as follows $y_{T+1} \cup y_{T+2} \cup y_{T+3} = (z_{1T}z_{2T+1} \cup z_{2T}z_{1T+1}) \cup (z_{2T}z_{3T+2} \cup z_{3T}z_{2T+2}) \cup (z_{1T}z_{3T+3} \cup z_{3T}z_{1T+3})$. These six possible transitions are depicted by the dotted lines in Fig. 6. Further, when applying the same concept during each time $0 \leq \boldsymbol{k} \leq \boldsymbol{\mathcal{K}}$ and aggregating all the results, this will lead to a complete transition delay model.

The delay model is described as follows:

$$\forall\, i\epsilon\mathcal{N}_s, k\epsilon\mathcal{N}_k \begin{cases} \sum_i z_{ik} = 1 & (3) \\ \frac{\sum_i \sum_k |z_{ik} - z_{ik-1}|}{2} \leq N_{trips} & (4) \\ \mathbb{Y} = \{y_1, y_2, y_k \dots, y_{\mathcal{K}}\} & (5) \end{cases}$$

Equation (3) states that the MESS truck can only be at one station $i$ at any sample $k$. In case of multiple MESS units, the right-hand side of (3) is replaced by $N_{mess}$ which is the total number of MESS trucks; this case will be investigated in future studies. Equation (4) constraints the maximum number of trips that MESS can make per day ($N_{trips}$) which equals half the number transitions. In case the MESS moved at time $k$ from a station $i$ to be at station $j$, then $z_{ik} = 0, z_{ik-1} = 1, z_{jk} = 1, z_{jk-1} = 0$ and the sum of the difference at sample $k$ is calculated as $\sum_i \frac{|z_{ik} - z_{ik-1}|}{2} = 1$, which means one trip is made. However, if the MESS stays at station $i$ at samples $k$ and at $k$-1, then $\sum_i \frac{|z_{ik} - z_{ik-1}|}{2} = 0$ which means no trips are made. Finally, (5) is a set of equalities that represent the transit flag $y_k$.

### B. Power Flow Model

Second, the system power flow is a model that links a set of buses $b\epsilon\mathcal{N}_b$ by a set of branches $t \in \mathcal{N}_t$. Buses active and reactive power controls buses angles and voltages. Apparent power at each bus is represented as the sum of RES, load, generators, and MESS powers injected at the bus (if any exists). The apparent power is decomposed into active and reactive power, expressed at (6) and (7).

$$p_{bk} = p_{lk} + p_{sk} - p_{gk} - p_{rk} \quad (6)$$

$$q_{bk} = q_{lk} + q_{sk} + q_{gk} + q_{rk} \quad (7)$$

$$\forall b = s = g = l = r, b\epsilon\mathcal{N}_b, s\epsilon\mathcal{N}_s, k\epsilon\mathcal{N}_k, l\epsilon\mathcal{N}_l, r\epsilon\mathcal{N}_r, g\epsilon\mathcal{N}_g$$

For each branch $t$ (line or transformer) that links two buses $(a, b)$ or $t\epsilon\mathcal{N}_t, t = (a, b)$, the branch complex impedance is calculated as $z_t = r_t + jx_t$, where $r_t$, $x_t$ is the branch resistance and reactance, respectively. The power flow for each branch is modelled in (8)-(13) as given in [33]. These equations do not include the angle of voltage with the assumption that no big change in voltage angle occurs in the distribution system [34]. It is worth mentioning that the voltage equation in (10) is not applicable at the slack bus ($b=0$) because it is a voltage controlled bus with a reference angle.

$$\forall t\epsilon\mathcal{N}_t, k\epsilon\mathcal{N}_k \begin{cases} p_{bk} = \mathcal{p}_{tk} - r_t\ell_{tk} - \sum_{\forall h\epsilon\mathcal{N}_t, h=(a,b), a\epsilon\mathcal{N}_b} \mathcal{p}_{hk} & (8) \\ q_{bk} = q_{tk} - x_t\ell_{tk} - \sum_{\forall h\epsilon\mathcal{N}_t, h=(a,b), a\epsilon\mathcal{N}_b} q_{hk} & (9) \\ v_{bk} = v_{ak} - 2(r_t\mathcal{p}_{tk} + x_t q_{tk}) + (r_t^2 + x_t^2)\ell_{tk} & (10) \\ \ell_{tk} = \frac{\mathcal{p}_{tk}^2 + q_{tk}^2}{v_a} & (11) \\ \ell_{tk} = |I_{tk}|^2 \quad , t = (a, b) & (12) \\ v_{bk} = |V_{bk}|^2 & (13) \\ loss_k = \sum_{\forall t\epsilon\mathcal{N}_t} r_t\ell_{tk} & (14) \end{cases}$$

In (8)-(14), $\mathcal{p}_{tk}, q_{tk}, I_{tk}, \ell_{tk}, V_{bk}, v_{bk}, loss_k$ are the branch $t$ active and reactive power; the magnitude of the line current; the second norm of the line current; the bus voltage; the second norm of bus voltage; and the total power losses, respectively. All these variables are measured at time sample $k$. Equations (8) and (9) express the active, reactive power balance equation for each branch $t$ at time $k$. Equation (10) represents the Ohm's law used to calculate the voltage drop in each branch. Equation (11) is the power flow equation that calculates each branch current from its apparent power. Equations (12) and (13) show that the used values for the power flow are the second norm for the voltage and branch currents. Finally, the power loss is calculated in (14). The main power flow constraints are the branches thermal limit expressed in (15) and the voltage level limit expressed in (16).

$$\forall b\epsilon\mathcal{N}_b, t\epsilon\mathcal{N}_t, k\epsilon\mathcal{N}_k \begin{cases} \ell_{tk} \leq \overline{\ell}_t & (15) \\ \underline{v} \leq v_{bk} \leq \overline{v} & (16) \end{cases}$$

### C. ESS Dynamic Model

The final part of the technical model is the ESS dynamics including the ESS power, total number of cycles $N$, and the state of charge ($SOC$) which are expressed in (17)-(19).

In this model, we assume that anytime, there is always an ESS at each station $s$; however, the constraint in (3) states that the MESS can be located at one unique station. Thus, the condition for injecting discharge ($p_{dh_{sk}}$) or importing charge power( $p_{ch_{sk}}$) at a certain bus $s$ at time $k$ is that the MESS exists at this station ($z_{sk} = 1$), and the MESS is not at transit state ($y_k = 0$). These conditions are modelled by (17). Equation (18) expresses the SOC as an integrator. The SOC equals one if the accumulated charge reaches the rated energy of the storage $\overline{E}_s$. The charge and discharge efficiency is considered as $\eta_{ch}, \eta_{dh}$, respectively. As one MESS is assumed at each bus, the total SOC is the sum of all stations ESS SOC at a certain time. A similar technique is used for calculating the number of cycles $N_k$ that is assumed as an integrator as well.

The number of cycles is incremented by one each time a full charge is absorbed by the MESS and injected again to the grid as expressed in (19).

$$\begin{cases} p_{sk} = (p_{ch_{sk}} + p_{dh_{sk}}) z_{sk}(1 - y_k) & (17) \\ SOC_{k+1} = \sum_s SOC_{sk} + \frac{T_s}{\overline{E}_s}(\eta_{ch} p_{ch_{sk}} + \eta_{dh} p_{dh_{sk}}) z_{sk}(1 - y_k) & (18) \\ N_{k+1} = \sum_s N_{sk} + \frac{T_s(p_{ch_{sk}} - p_{dh_{sk}})}{2\overline{E}_s} z_{sk}(1 - y_k) & (19) \end{cases}$$

$$\forall k\epsilon\mathcal{N}_k, s\epsilon\mathcal{N}_s, \eta_{ch} < 1, \eta_{dh} > 1$$

This article has been accepted for publication in a future issue of this journal, but has not been fully edited. Content may change prior to final publication. Citation information: DOI 10.1109/TIE.2017.2682779, IEEE Transactions on Industrial Electronics



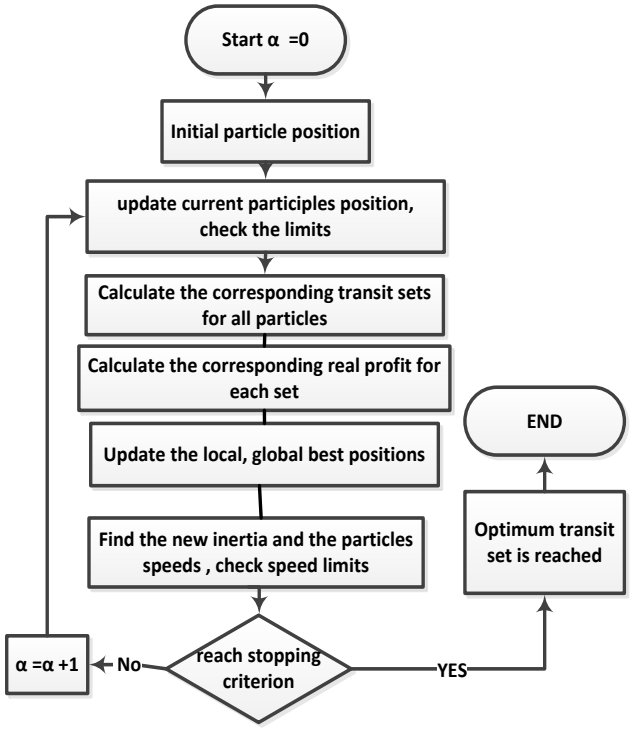


Fig. 7. Stage 2 structure (PSO profit maximizer).

The dynamic ESS constraints are stated in (20)-(24). While constraints (20) and (21) define the charge and discharge powers as positive and negative power limited by the thermal limit of the MESS, constraint (22) limits the apparent power of the MESS to be upper bounded by the rated MESS apparent power ($\bar{s}$) at any time. Finally, the SOC is limited in (23) between the desired minimum SOC $\underline{SOC}$ and one to avoid deep discharge and overcharging that may reduce the battery life dramatically. Further, the number of cycles at the end of the day is limited by (24) as the battery life is a countable number of cycles.

$$0 \le p_{ch_{sk}} \le \bar{p}_s \tag{20}$$

$$-\bar{p}_s \le p_{dh_{sk}} \le 0 \tag{21}$$

$$p_{sk}^2 + q_{sk}^2 \le \bar{S} \tag{22}$$

$$\underline{SOC} \le SOC_k \le 1 \tag{23}$$

$$N_{\mathcal{K}} \le \bar{N} \tag{24}$$

$$\forall\, b\epsilon\mathcal{N}_b, t\epsilon\mathcal{N}_t, k\epsilon\mathcal{N}_k$$

### D. Original EMS Problem

The EMS objective is maximizing the day-ahead profit for the DNO by minimizing the imported energy cost from the grid (energy arbitrage). It is assumed that the MESS is an asset owned by the DNO to provide both reactive power support and maximize net profit. RESs are owned by different parties, and they are paid a fixed feed-in-tariff (FIT) as a motivation by the government for clean energy, such a case exists in several markets, such as Ontario, Canada [35]. RESs are operated according to the maximum power point tracking strategy; the DNO buys this energy from RESs owners with the regulated FIT ($C_{FIT}$) . The day-ahead cost of buying RESs energy is given in (26). On the other hand, conventional distributed generators (DGs) owned by the DNO, such as microturbines or diesel engines, have an operating cost ($C_{DG}$). A quadratic cost function, as defined in (25), precisely represents the operation costs of DG units [33]. In (25), $\phi_g\$/(kWh)^2, \beta_g(\$/kWh), \gamma_g(\$)$ are constants that depend on the generator type.

$$C_{DG} = \sum_{k=1}^{\mathcal{K}} \sum_{g=1}^{\mathcal{G}} \phi_g \left(p_{gk} T_s\right)^2 + \beta_g \left(p_{gk} T_s\right) + \gamma_g \tag{25}$$

$$C_{res} = \sum_{k=1}^{\mathcal{K}} \sum_{r=1}^{\mathfrak{R}} p_{rk} T_s C_{FIT} \tag{26}$$

The MESS cost $C_{mess}$ includes both the truck operating cost $C_{truck}$ and the ESS cost $C_{ess}$ as in (27). Firstly, the truck operating cost (28) includes a fuel cost and labor cost. While the fuel cost is modelled as a worst case cost (the multiplication of maximum distance (in km) by the number of the trips by the fuel consumption cost $FC$ ($\$/km$)), the truck labor cost $tlc$ includes the daily stipend of the truck driver and technicians. Secondly, (29) models the ESS cost as a levelised cost ($C_{kwh}\$/kWh\, charged$). This cost is adopted before for ESS in [36]. However, the capital cost is modified to include the truck capital cost and ESS maintenance cost that includes the truck maintenance cost; further details on MESS cost calculations are available but omitted here for space limitations.

$$C_{mess} = C_{truck} + C_{ess} \tag{27}$$

$$C_{truck} = FC \times N_{trip} \times \max(Dist) + tlc \tag{28}$$

$$C_{ess} = \sum_{k=1}^{\mathcal{K}} \sum_{s=1}^{s} P_{ch_{sk}} T_s C_{kwh} \tag{29}$$

The final cost item is the grid power cost $C_{grid}$ that is the multiplication of the expected pool price (buy price) $BP_k(\$/kWh)$ and the grid energy $P_{gridk} T_s$ as shown in (30). This cost has a negative value (becomes income) in case the distribution system exports surplus energy to the grid. The income of the DNO is generated from daily selling energy to the loads with the sell price $SP_k(\$/kWh)$ as given in (31).

Finally, the profit is the difference between the income and the costs (MESS operating cost, DG running cost plus RES energy purchasing cost) as shown in (32).

$$C_{grid} = \sum_{k=1}^{\mathcal{K}} T_s BP_k P_{gridk}, P_{gridk} = P_{bk}, b = 0 \tag{30}$$

$$inc = \sum_{k=1}^{\mathcal{K}} \sum_{l=1}^{\mathcal{L}} T_s SP_k P_{lk} \tag{31}$$

$$pro = inc - C_{grid} - c_{mess} - C_{DG} - C_{res} \tag{32}$$

The final optimization problem is expressed as follows

$$\max_{p_{ch_{sk}}, p_{dh_{sk}}, \mathbb{Z}, q_{sk}} (pro)$$
$$S.t.\ \ (3)-(11), (15)-(24) \tag{33}$$

The problem in (33) is a mixed integer nonconvex problem that faces a feasibility problem. In Section IV, this problem will be converted to a mixed integer second-order cone problem (MISOCP) using the proposed two-stage EMS.

## IV. Two-stage EMS

To convert the problem in (33) into a mixed integer convex problem, the following suboptimal two-stage solution is proposed. Firstly, the problem is solved assuming instantaneous MESS transit; this problem calculates the MESS designated stations and its transit times (given the previous assumption).

Secondly, a particle swarm algorithm optimizes the transit times of the first stage without changing the MESS stations.

### A. Stage 1 (Instantaneous Transit EMS)

The delay model $\mathbb{Y}$ given in (5) is a nonlinear sophisticated Boolean expression that depends on both the truck transit time and stations $\mathbb{Z}$. Assuming that $\mathbb{Y}=0$ or MESS can move instantaneously from a station to another will reduce the problem complexity on the price of sub-optimality, this part will be discussed in Section IV.B. Even with the assumption $\mathbb{Y}=0$, the problem (33) is still nonconvex problem due to nonconvex equality constraints in the power system (11) and ESS model (17)-(19).

For the power system power flow model (11), according to [33], it can be relaxed to the inequality (34) given the following two sufficient assumptions. Firstly, the bus voltage deviation is not too large. Secondly, the buses generated powers are not too large. These conditions are usually satisfied in typical distribution systems. The quadratic constraint (34) is equivalent to the second-order cone constraint in (35) [37].

$$\ell_{tk} v_a \geq \mathcal{p}_{tk}^2 + q_{tk}^2 \forall t \epsilon \mathcal{N}_t, k \epsilon \mathcal{N}_k, t=(a,b) \tag{34}$$

$$\left\| \begin{matrix} 2\mathcal{p}_{tk} \\ 2q_{tk} \\ \ell_{tk}-v_a \end{matrix} \right\|_2 \leq \ell_{tk}+v_a \tag{35}$$

The ESS model (17)-(19) is expressed as a linear set of equalities as in (36)-(38). This is possible after modifying the power limits constraints from (20)-(21) into (39)-(40) and adding a reactive power constraint (41). This simple modification states that the MESS can charge or discharge at any station and time (s, *k*) if and only if it exists at this station or $z_{sk}=1$. Otherwise, the power limits is set to zero. These limits affect all ESS dynamics as given in (36)-(38).

$$\begin{cases} p_{sk} = p_{ch_{sk}} + p_{dh_{sk}} & (36) \\ SOC_{k+1} = \sum_s SOC_{sk} + \dfrac{T_s}{\bar{E}_s}\left(\eta_{ch} p_{ch_{sk}} + \eta_{dh} p_{dh_{sk}}\right) & (37) \\ N_{k+1} = \sum_s N_{sk} + \dfrac{T_s(\eta_{ch} p_{ch_{sk}} - \eta_{dh} p_{dh_{sk}})}{2\bar{E}_s} & (38) \\ 0 \leq p_{ch_{sk}} \leq \bar{p}_s z_{sk} & (39) \\ -\bar{p}_s z_{sk} \leq p_{dh_{sk}} \leq 0 & (40) \\ -\bar{s} z_{sk} \leq q_{sk} \leq \bar{s} z_{sk} & (41) \end{cases}$$

Now, the instantaneous EMS problem is expressed as

$$\max_{p_{ch_{sk}}, p_{dh_{sk}}, \mathbb{Z}, q_{sk}} (pro) \tag{42}$$

$$S.t. \begin{cases} instaneous\ transit\ model: (3),(4) \\ power\ flow\ model: (6)-(10),(15)-(16),(35) \\ ESS\ model: (22)-(24)\&(36)-(41) \end{cases}$$

Now, the problem in (42) is a mixed-integer SOCP problem that is solved efficiently using the available commercial solvers, such as GUROBI [38]. It is worth mentioning that problem (42) represents a finite-horizon model predictive control problem, because the overall system is aggregated as a single state-space dynamic model. At each sample time $0 \leq \boldsymbol{k} \leq \boldsymbol{\mathcal{K}}$, the model is regressively used to derive the future outputs as a function in the model expected states and the future control action along the prediction horizon [39]. The inputs of the state-space model are the MESS power and locations $[z_{ik}, p_{sk}, q_{sk}]$, whereas the system states are the SOC and number of cycles $[SOC_{sk}, N_{sk}]$. Finally, the controlled outputs are any constrained variable in the system such as $[SOC_k, N_k, p_{sk}, q_{sk}, \mathcal{p}_{tk}, \dots]$.

### B. Stage 2 (PSO Profit Maximizer)

The resulting profit from Stage 1 is not the actual profit. In reality, MESS transit period is not zero, and every time the MESS moves from a station $i$ at instant $\lambda$ heading to another station $j$, it will stay in transit for a period $\tau_{ijk}$ defined by (2) till it reaches its destination at instant $\lambda+\tau_{ij\lambda}$. The set of time indices that define that the MESS is at transit state is $\mathcal{N}_\tau$:

$$\mathcal{N}_\tau = \{[\lambda, \lambda+\tau_{ij\lambda}] | z_{i\lambda} = z_{j\lambda-1} = 1 \forall i \neq j, i, j \in \mathcal{N}_s, \lambda \epsilon \mathcal{N}_k\} \tag{43}$$

Now, if the MESS is at transit, that means that the DNO has to buy (or sell) the MESS scheduled energy from the grid till the MESS reaches its next destination. Further, the MESS is not operating during transit periods, thus its operating cost $C_{ess}$ should not be considered as well. The real profit $\mathcal{R}pro$ when the transit set $\mathcal{N}_\tau$ is taken into account is;

$$\mathcal{R}pro = pro + \sum_{\lambda \epsilon \mathcal{N}_\tau} \sum_{s \in \mathcal{N}_s} T_s BP_\lambda p_{s\lambda} + \sum_{\lambda \epsilon \mathcal{N}_\tau} \sum_{s \in \mathcal{N}_s} P_{ch_{s\lambda}} T_s C_{kwh} \tag{44}$$

It is worth mentioning that if $p_{s\lambda} < 0$, which means the MESS is discharging at this time; however, as the MESS is in the transit state, this energy $\sum_{s \in \mathcal{N}_s} T_s p_{s\lambda}$ is exported from the grid with a price $BP_\lambda$ at this time. On the contrary, if the MESS is supposed to be charged at this time, the surplus system energy is sold to the grid with this time price (or even worse, RESs energy can be curtailed in case the voltage level or thermal current levels are violated). Further, the ESS cost is excluded from the profit calculation during time periods flagged in $\mathcal{N}_\tau$. Not only, is the profit and power system is affected by the delay, but also the ESS dynamics as well. For instance, the real SOC ($\mathcal{R}SOC$) after considering the transit delay is defined as in (45) (where $p_{ch_{sk}}, p_{dh_{sk}}$ are calculated by (42)). As shown in (45), the SOC is normally calculated in the non-transit case, while it stays fixed during transit as the ESS is in the stand-by mode. Other ESS dynamics, such as the real number of cycles $\mathcal{R}N$ is calculated as in (46).

$$\begin{cases} \mathcal{R}SOC_{k+1} = \sum_s \mathcal{R}SOC_{sk} + \dfrac{T_s}{\bar{E}_s}\left(\eta_{ch} p_{ch_{sk}} + \eta_{dh} p_{dh_{sk}}\right), k \in \mathcal{N}_k - \mathcal{N}_\tau \\ \mathcal{R}SOC_{k+1} = \mathcal{R}SOC_k, k \in \mathcal{N}_\tau \end{cases} \tag{45}$$

$$\begin{cases} \mathcal{R}N_{k+1} = \sum_s \mathcal{R}N_{sk} + \dfrac{T_s(\eta_{ch} p_{ch_{sk}} - \eta_{dh} p_{dh_{sk}})}{2\bar{E}_s}, k \in \mathcal{N}_k - \mathcal{N}_\tau \\ \mathcal{R}N_{k+1} = \mathcal{R}N_k, k \in \mathcal{N}_\tau \end{cases} \tag{46}$$

One needs to make sure that the transit set will not lead to ESS dynamic constraint violation. For instance, one transit set can move the MESS very early from discharge stations and very late from charging station, thus an overcharge may occur and vice versa. One solution to this problem is keeping a reserve in the capacity (e.g., the SOC limits are chosen from 20 to 90 %) to account for possible uncertainties.

The PSO optimizer defines optimum transit delay set $\mathcal{N}_\tau$ that maximizes the real profit without violating the ESS dynamics. Firstly, each particle $x^n$ represents a different transit set $\mathcal{N}_\tau^n$ by changing the transit time $\lambda_\alpha^n$, where *n* is the index for the particle in the population, and $\alpha$ is the index for the transit time. Normally, the number of transits is less than or equal $N_{trips}$

$$x^n = [\lambda_1^n, \lambda_2^n, .., \lambda_{N_{trips}}^n] \tag{47}$$

$$\mathcal{N}_\tau^n = \{[\lambda_1^n, \lambda_1^n + \tau_{ij\lambda_1^n}], [\lambda_2^n, \lambda_2^n + \tau_{ij\lambda_2^n}] .. [\lambda_{N_{trips}}^n, \lambda_{N_{trips}}^n + \tau_{ij\lambda_{N_{trips}}^n}]\} \tag{48}$$

$$\lambda_\alpha - M \leq \lambda_\alpha^n \leq \lambda_\alpha + M, 1 \leq \alpha \leq N_{trips} \tag{49}$$

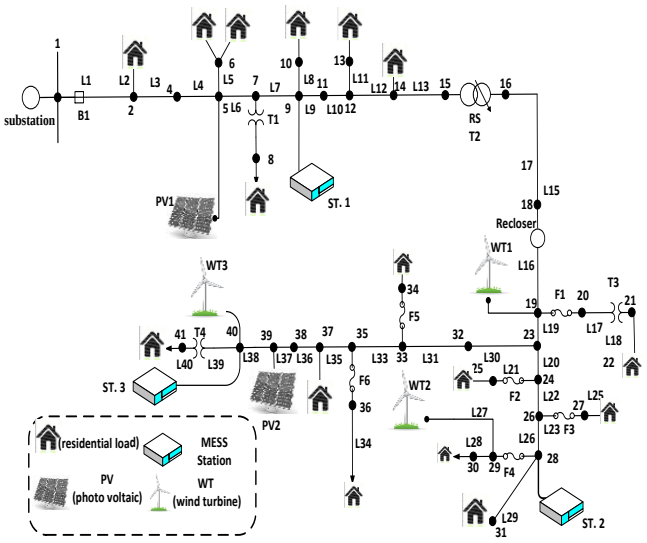


Fig. 8. Radial feeder under study.

As shown, the particle $x^n$ is a randomly generated vector for the transit and is bounded by that defines the maximum shift in the transit time within a band $[-M, M]$. The swarm population $\mathbb{X}$ is then defined with a population-size $n$ particles, each has a corresponding transit set defined in (51) .

$$\mathbb{X} = \{x^1, x^2 \dots x^n \dots x^n\} \tag{50}$$

$$\mathbb{N} = \{\mathcal{N}_\tau^1, \mathcal{N}_\tau^2 \dots \mathcal{N}_\tau^n \dots \mathcal{N}_\tau^n\} \tag{51}$$

The real profit is calculated for each particle, and the local and global best particle positions are allocated. At each iteration $\alpha$, after the profit is calculated for all $\mathbb{x}$ set-particles, the local and global best positions $Pbest(\alpha), G_{best}(\alpha)$ are updated and the new velocity for the next sample ($V^n(\alpha+1)$) for each particle $n$ is calculated as in (53). For solution quality, the PSO algorithm must fulfill two important criteria: first, a high exploration at the start of the search, and second, a deep exploitation to avoid trapping in a local-suboptimal later [40]. Thus, a high speed for particles exploration is gained via high initial inertia that reduces monotonically with the iterations progress in order to achieve higher exploitation later. This is possible by updating the PSO inertia $\omega(\alpha)$ as in (52), starting from the desired minimum value $\omega_{min}$ at the first search sample and reaching its peak $\omega_{max}$at the maximum iteration value $Max.Iter$. Next, the particles positions are updated as in (54). The reader is referred to [40] for further details on the PSO algorithm. Finally, the stopping criterion is achieved in two cases. Firstly, the convergence case happens if the fitness function (real profit) settles at a certain value within the predefined tolerance zone.

$$\omega(\alpha) = \omega_{max} - \frac{\omega_{max} - \omega_{min}}{Max.Iter}\alpha \tag{52}$$

$$V^n(\alpha+1) = \omega(\alpha)V^n(\alpha) + c_1 r_1\big(Pbest - x^n(\alpha)\big) + c_2 r_2\big(Gbest - x^n(\alpha)\big) \tag{53}$$

$$x^n(\alpha+1) = V^n(\alpha+1) + x^n(\alpha) \tag{54}$$

This must happen for a predefined number of iterations to guarantee convergence and avoid trapping in a local minimum. Secondly, the stopping criterion in satisfied if the number of iterations exceeds the maximum iteration numbers ($\alpha \leq \overline{\alpha}$). Fig. 7 shows the PSO algorithm structure.

## V. Case Study

To validate the proposed EMS, a detailed simulation study is conducted on a 41-bus real radial feeder in Ontario, Canada [41]. The distribution feeder is rated at 16.185 MVA and has a medium voltage 16 kV. The feeder has five RESs (three wind turbines (WTs) and two photovoltaic (PV) generators) with a gross penetration of 37% (6.0 MVA). The feeder has 40 branches and extends for 30 kilometers [41]. The feeder data details, including the lines impedance, lengths and each bus nominal load, are given in [41]. The daily load profile follows the IEEE RTS model derived using three years load data for this feeder [41], and it is shown in Fig. 9(a). On the other hand, typical RESs profiles, shown in Fig. 7(b), are taken from the typical historical data provided in [26]. The rated powers of RESs are given in Table I. In Ontario, Canada, the largest power distribution utility, Hydro One, has a fixed electricity tariff to its customers that only changes only from winter to summer [42].

The tariff adopts the time-of-use pricing policy with two peaks periods (7:11 am, 5:7 PM). Other rates such as delivery rates, regulatory charges are considered here as well [42]. On the other hand, the DNO (here Hydro One) buys energy from Ontario independent system operator ISO (IESO) for the wholesale energy market price (deregulated market). This price is known as hourly Ontario energy price (*HOEP*) [43]. The real HOEP in February 2015 is considered here as given in [43]. The HOEP and DNO tariff (buy and sell prices) are shown in Fig. 9(c). RESs owners are paid a feed-in-tariff ($c_{FIT}$) decided by IESO as given in [44], and it is given in Table I. No utility-owned DGs exist in the system under study; however, DGs can be easily dispatched by considering their active and reactive power limits, and, power rate constraints as detailed in [33].

The MESS optimal sizing is conducted similar to the one adopted in [45], the storage cost is 600 K$/MWh and the conversion system cost is 350k$/MW [46], while the operation and maintenance cost for MESS is assumed to be 12k$/year including the ESS and the truck, the truck sot is assumed to be 50k$.

The MESS is assumed to participate 250 cycles/year with results in a 3000 cycle per its life time (here 12 years), thus not replacement cost is assumed. After making stochastic sizing using these input data, an optimal size of MESS is found to be 3250 kVA/6381.3 kWh which equals 4.247 Million $. The MESS efficiency and cost parameters are stated in Table I. The ESS allocation technique for reducing RESs spilled energy, given in [41], is adopted as a candidate set for optimal MESS stations. Using a similar technique as in [45] results in three optimal stations at buses (station-1 at bus 9, station-2 at bus 28, and station-3 at bus 40). It is worth mentioning that the resulting positions are at each feeder end (where high voltage drop occurs) representing perfect candidates to provide reactive power support. The distance between different stations is given in Table I. Finally, for the MESS delay model, the traffic congestion delay is used to emulate the traffic congestion pattern in freeway of a large North American city. Although the traffic events and the scheduled road maintenance are given on a real-time basis for Ontario Canada from [47], the exact transit delay data in Ontario is not available for public. As a result, this

This article has been accepted for publication in a future issue of this journal, but has not been fully edited. Content may change prior to final publication. Citation information: DOI 10.1109/TIE.2017.2682779, IEEE Transactions on Industrial Electronics



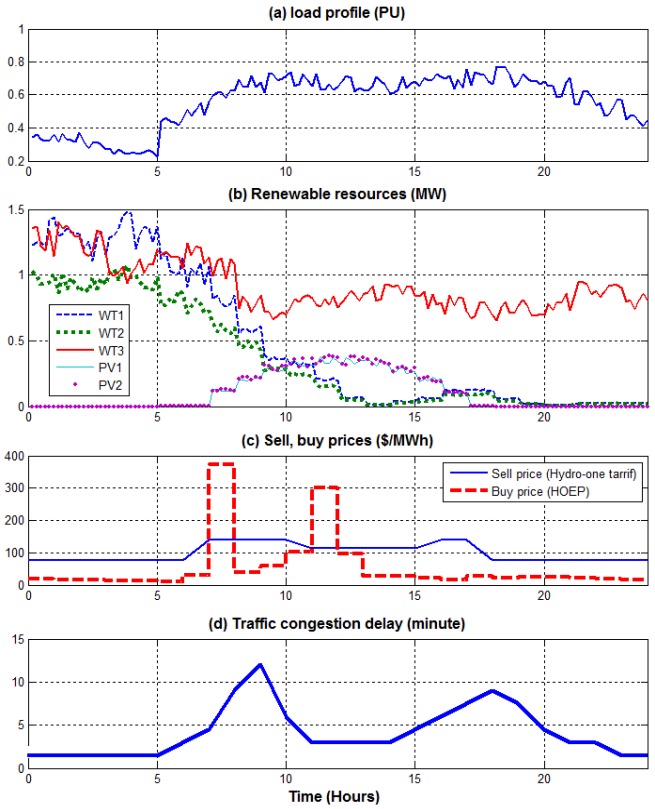


Fig. 9. Day-ahead input data. (a) Load profile. (b) RESs profiles. (c) Wholesale market and sell prices. (d) Traffic congestion delay.

Table I. Input data for the EMS.

| | |
|---|---|
| RES Ratings | $p_{WT1} = 2MW, p_{WT2} = 1.5MW, p_{WT3} = 1.5MW,$ $p_{pv1} = 0.5MW, p_{pv2} = 0.5MW, c_{FIT} = 128\ \$/MWh$ |
| Delay model | $d_{12} = 16.87\ Km, d_{13} = 19.92\ Km, d_{23} = 16.83\ Km$ $V_{avg} = 40\ {}^{Km}/_{hr}, t_{ins} = 5\ mins., T_s = 10\ mins.$ |
| EMS | $SOC_0 = 0.5, \underline{SOC} = 0.2, N_{trips} = 3, \overline{N} = 1$ $\underline{v} = 0.95, \overline{v} = 1.05, N_0 = 0, \eta_{ch} = 0.75, \eta_{dh} = 1.33$ $FC = 0.4\ {}^{\$}/_{Km}, C_{kwh} = 221\ {}^{\$}/_{MWh}, tlc = 25\ {}^{\$}/_{hr}$ |
| PSO | $M = 30\ mins., \omega_{max} = 0.9, \omega_{min} = 0.1, \overline{\alpha} = 2000,$ $C_1 = 2, C_2 = 2, n = 10$ |

case study uses the transit delay data of Los Angeles, USA, given in [48], as a sample of the traffic congestion pattern in freeways in large North American cities. The data is represented in Fig. 9(d). In case the DNO has an estimation for the transit delay, then the EMS problem is solved as instant transition EMS problem and a suboptimal solution can be obtained.

For the given system inputs shown in Fig. 9, the EMS problem (42) is solved, and the results are shown in Fig. 10, whereas the voltage profile after and before using the MESS is depicted in Fig. 11. The main objective is maximizing the DNO profit through energy arbitrage and power losses minimization; thus as shown in Fig. 10 (b), the MESS has been charged during the lowest buy prices times (4-6 am) till reaching full capacity.

The MESS is partially discharged during the first price peak at 8 am. It continues being charged at 9 am when the prices fall. It is worth mentioning that at 9 am, the battery is not charged with full power as reactive power support is needed at this time to boost the voltage to the minimum allowable level as depicted in the reactive power curve in Fig. 10(b). Next, at the noon, where the second price peak exists, the MESS is fully discharged. After that, no significate price difference exists that deserves another MESS charge and the state of charge is settled at the minimum 20% level as in Fig. 10(d). It should be noted that the price difference should be at least greater than the charging cost $C_{kwh}$ to make charging economically viable (which does not happen again after 2 pm). Moreover, the number of cycles allowed in this study is one; thus the total charged energy is less than the rated capacity and the maximum number of cycle is less than one as in Fig. 10(d). Finally, as the profit is the only objective function here (energy arbitrage strategy), charging times are driven by the energy price, unlike peak shaving whereas discharging hours are always located at peak hours. It is noticed that the grid exported power is reduced during the high energy price as depicted in Fig. 10(c).

Regarding reactive power support, during late night, the power generated by wind turbines is very high while the line is lightly loaded (see Fig. 9). As a result, the voltage profile increases above the limits (105%) during this time as shown in Fig. 11, especially at the feeder end (bus 41). As a result, the first chosen location for the MESS is near these buses (station-3) as shown in Fig. 10(a). During this time the energy price is minimal and the MESS is fully charged. In the morning (7-8 am), the MESS discharge during the first peak hour, and then it changes its location to station-1 (bus 9) where it recharges back (8-9 am). The reason behind this location change is that charging at station-1 (the nearest to grid) provides the lowest power losses, further charging at station-3 (bus 40) will lead to a further voltage drop at the feeder's end. The second transition occurs after charging as shown in Fig. 10(a), when the MESS goes back to station-3 (bus 40) to discharge fully during the second peak hour (11 am-12 pm). After that, the SOC and number of cycles limits are reached as shown in Fig. 10(d), thus zero active power is kept till the end of the day, however; the MESS keeps providing reactive power support for keeping an acceptable voltage limits. A final transition is made to station-2 around 2 pm. As noticed from Fig. 9, the wind power plant (WT2) near station-2 drops to zero at the same time; thus a leading reactive power is needed at this far end feeder. Thus, the MESS made this final transition from station3 into station 2 where the voltage to reactive power sensitivity is is higher than station-3.

Regarding Stage 2 (the PSO profit maximizer), the optimizer changes the transition time from (8, 9 and 14) into (8&9:30 and 13:30). For the first and second transitions, the PSO keeps them the same as if MESS left station-3 earlier than 8, it will miss discharging during the peak hour which will result in a big profit reduction. For the second transition, if MESS left station-1 before 9 am, it will not be fully charged which will reduce the profit in the future, however, if it stayed longer at station-1, the traffic congestion delay will reduce from its 9 am peak as depicted in Fig. 7(d). Finally, for the final transition (from station 3 into station 2), the PSO optimizer changes the transition time from (2 pm into 1:30 pm) to end the ride (approximately 30 minutes ride with delays) from before the traffic congestion increases after (2 pm). It is worth mentioning that the PSO results agree with the traffic delay profile in Fig. 9(d); thus, the PSO optimizes the transition times to decrease the MESS delay and, therefore, maximizing its service period.

To sum up the results, Table II compares the techno-economic aspects after and before using the MESS services (system with

This article has been accepted for publication in a future issue of this journal, but has not been fully edited. Content may change prior to final publication. Citation information: DOI 10.1109/TIE.2017.2682779, IEEE Transactions on Industrial Electronics



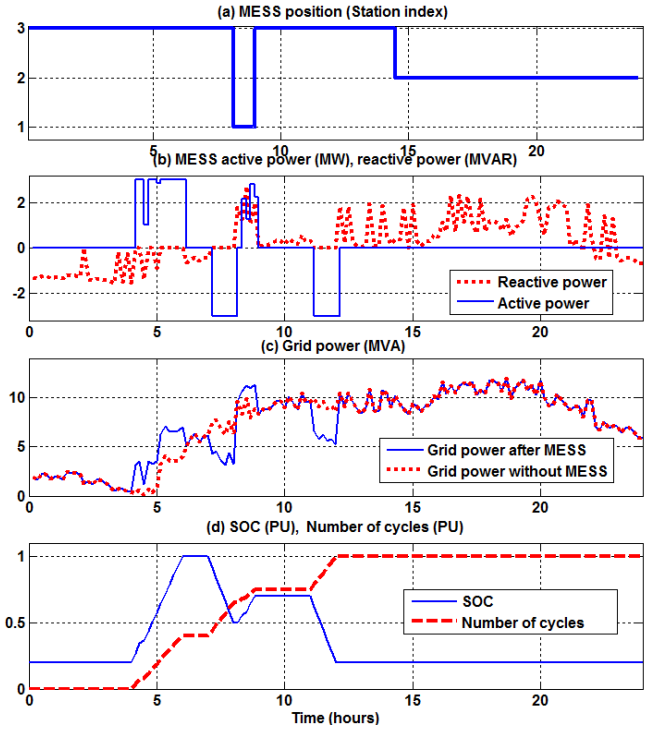


Fig. 10. EMS results (a)MESS Position (b) MESS active power and reactive power set (c) Grid power and (e) SOC and Number of cycles.

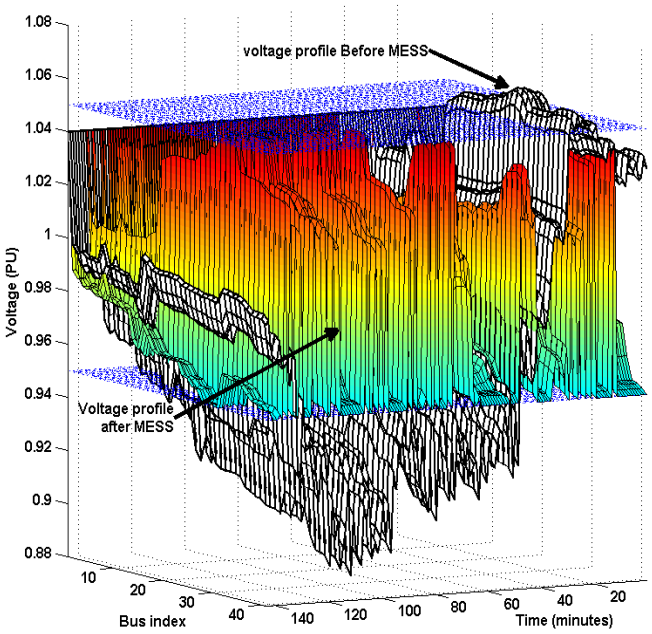


Fig. 11. Voltage profile after and before using the MESS.

no storage at all and system that invests in MESS). Firstly, the MESS managed to provide a logistic localized reactive power support to keep the voltage level within allowable limits which improves the power quality. Secondly, regarding losses, the losses has been decreased by 5.5%. It is worth mentioning that the objective function is the difference between the energy bought from the grid and that sold to loads. Thus the power losses is inherently minimized in the objective function with a weight depending the energy prices at each instant. Thirdly, the net profit has increased by 3.1% as compared to that without

Table II. System performance comparison.

| | Without MESS | With MESS |
|---|---|---|
| Voltage level | $V_{max} = 1.062, V_{min} = 0.89$ | $V_{max} = 1.04, V_{min} = 0.956$ |
| Power losses | 8.1863 $MWh$ | 7.7277 $MWh$ |
| Profit | 14,320$ | 14,760$ |

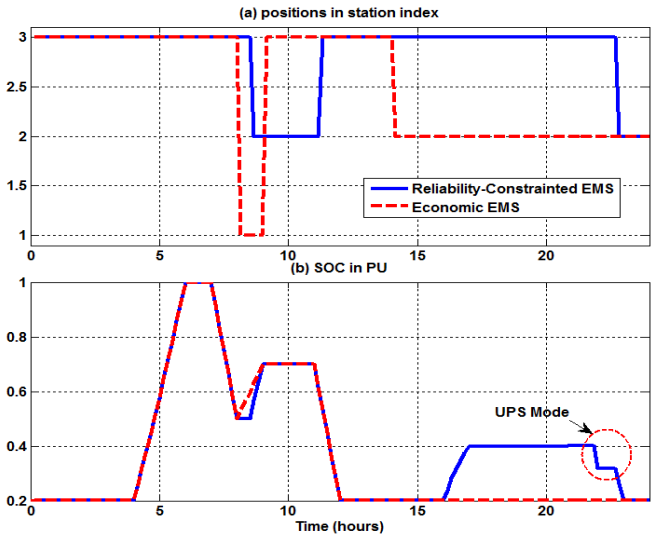


Fig. 12. Comparison between reliability-based EMS with economic EMS. (a) Station position of MESS. (B) MESS state of charge.

including the profit from the localized reactive power support that defers adding one or two capacitor banks to this feeder.

The second case study discusses a very important issue which is boosting the power system reliability by providing an on-line backup energy reservoir for sensitive loads, here the MESS acts as an uninterruptible power supply (UPS). This is possible by solving the same economic EMS problem after imposing UPS constraints that guarantee that the MESS has enough energy (minimum SOC greater than the required energy) and the MESS is sited at the desired location. If a fault occurs, the MESS switches off into UPS mode till the service is continued again. The UPS constraints are summarized in (55-56).

$$\underline{SOC} + \frac{E_{UPS}}{\bar{E}_s} \leq SOC_k \leq 1 \quad \forall k \in [T_{ups}^{start}, T_{ups}^{end}] \tag{55}$$

$$z_{sk} = z_{UPS} \tag{56}$$

The UPS constraints assume that the MESS is required to provide a reserve energy $E_{UPS}$ for a certain time period $[T_{ups}^{start}, T_{ups}^{end}]$ while locating the MESS at the position $z_{UPS}$.

The main case study is repeated but with the assumption that a critical load exists at station three from hours 17 till 23. The required energy reservoir is ($E_{UPS} = 1250$ kWh) which represents 20% of the battery capacity; thus the SOC should not go below 40% at the pre-mentioned hours. A comparison between the economic MESS and the resulting UPS constrained (after imposing constraints 55-56) is shown in Fig. 12.

In the UPS-constrained EMS, the MESS starts charging early to reach the required 40% SOC by hour 17. At time 21:50, the main supply is disconnected and the MESS starts acting as a UPS till the service is resumed by 22:40. When the MESS returns again to the normal mode after hour 23, it discharges the whole energy to go back to the minimum SOC of 20%. It is worth mentioning that the MESS also stayed at station-3 till

hour 23, then it moved to station-2 after (similar to the economic EMS case).

Finally, it worth noticing that these results mainly depend on the market prices, the load and RES profiles. Thus, in other days with no big market price difference, it is not economic to operate the MESS [49]. Finally, Using MESS in voltage support is optional in case of long feeders where the transformer tap-changer setting cannot guarantee an acceptable voltage at the far end.

## VI. Conclusion

A day-ahead EMS for an MESS has been presented in this paper. The EMS objective function aims at maximizing the DNO day-ahead profit and regulating the voltage level. The proposed EMS dispatches the MESS and allocates its station in the system. A traffic delay model has been developed between different stations. Using a two-stage optimization technique, firstly, the problem is solved as a mixed-integer convex problem, and secondly, a PSO-based algorithm has been developed to optimize the transit times to maximize the profit. A case study on a real 41-buses radial feeder with real data of RESs and loads is used to validate the results. The proposed EMS has successfully fulfilled all the optimization process objectives in an adaptive manner that fits the time-varying nature of renewable resources in modern active distribution grids.

## References


[1] J. Sexauer and S. Mohagheghi, "Voltage Quality Assessment in a Distribution System With Distributed Generation—A Probabilistic Load Flow Approach," *IEEE Trans. Power Del.*, pp. 1652 - 1662, July 2013.

[2] G. C. Jim Eyer, "Energy Storage for the Electricity Grid: Benefits and Market Potential Assessment Guide," SANDIA , Albuquerque, New Mexico, 2010.

[3] J. A. Rahul Walawalkar, "Market Analysis of Emerging Electric Energy Storage Systems," NETL, 2008.

[4] Y. Rebours, D. Kirschen, M. Trotignon and S. Rossignol, "A Survey of Frequency and Voltage Control Ancillary Services—Part I: Technical Features," *IEEE Tran. Power Syst.*, vol. 22, no. 1, pp. 250-357, 2007.

[5] J. Zhong and K. Bhattacharya, "Toward a competitive market for reactive power," *IEEE Trans. Power Syst.*, vol. 17, no. 4, pp. 1206-1215, 2002.

[6] S.-C. Wang and Y.-H. Liu, "A PSO-Based Fuzzy-Controlled Searching for the Optimal Charge Pattern of Li-Ion Batteries," *IEEE Trans. Indust. Electron.*, vol. 62, no. 5, pp. 2983- 2993, 2015.

[7] J. Trovao, V. Santos, C. Henggeler Antunes, P. Pereirinha and H. Jorge, "A Real-Time Energy Management Architecture for Multisource Electric Vehicles," *IEEE Trans. Indust. Electron.*, vol. 62, no. 5, pp. 3223-3233, 2015.

[8] X. Lu, K. Sun, J. Guerrero, J. Vasquez and L. Huang, "State-of-Charge Balance Using Adaptive Droop Control for Distributed Energy Storage Systems in DC Microgrid Applications," *IEEE Trans. Indust. Electron.*, vol. 61, no. 6, pp. 2804- 2815, 2014.

[9] F. G.-T. a. C. Bordons, "Optimal Economical Schedule of Hydrogen-Based Microgrids With Hybrid Storage Using Model Predictive Control," *I IEEE Trans. Indust. Electron.*, vol. 62, no. 8, pp. 5195 - 5207, AUGUST 2015.

[10] A. Chaouachi, R. M. Kamel, R. Andoulsi and K. Nagasaka, "Multiobjective Intelligent Energy Management for a Microgrid," *IEEE Trans. Indust. Electron*, vol. 60, no. 4, pp. 1688-1699, April 2013.

[11] W. Tushar, B. Chai, C. Yuen, D. Smith, K. Wood, Z. Yang and H. Poor, "Three-Party Energy Management With Distributed Energy Resources in Smart Grid," *IEEE Trans. Indust. Electron.*, vol. 62, no. 4, pp. 2487-2498, 2015.

[12] J. Talla, L. Streit, Z. Peroutka and P. Drabek, "Position-Based T-S Fuzzy Power Management for Tram With Energy Storage System," *IEEE Trans. Indust. Electron.*, vol. 62, no. 5, pp. 3061- 3071, 2015.

[13] Y. Liu, C. Yuen, N. U. Hassan, S. Huang, R. Yu and S. Xie, "Electricity Cost Minimization for a Microgrid With Distributed Energy Resource Under Different Information Availability," *IEEE Trans. Indust. Electron.*, vol. 62, no. 4, pp. 2571-2583, 2015.

[14] R. Yu, W. Zhong, S. Xie, C. Yuen, S. Gjessing and Y. Zhang, "Balancing Power Demand Through EV Mobility in Vehicle-to-Grid Mobile Energy Networks," *IEEE Trans. Indust. Informat.*, vol. 12, no. 1, pp. 79-90, 2016.

[15] K. W. Hu and C. M. Liaw, "Incorporated Operation Control of DC Microgrid and Electric Vehicle," *IEEE Trans. Ind Elect*, vol. 63, no. 1, pp. 202-215, 2016.

[16] W. Tushar, C. Yuen, S. Huang, D. B. Smith and H. V. Poor, "Cost Minimization of Charging Stations With Photovoltaics: An Approach With EV Classification," *IEEE Trans. Intell Trans Syst*, vol. 17, no. 1, pp. 156-169, 2016.

[17] P. Sanchez-Martin, G. Sanchez and G. Morales-Espana, "Direct Load Control Decision Model for Aggregated EV Charging Points," *IEEE Trans Power Syst.*, vol. 27, no. 3, pp. 1577-1584, 2012.

[18] R. J. Bessa and M. A. Matos, "Optimization Models for EV Aggregator Participation in a Manual Reserve Market," *IEEE Tran Power Syst*, vol. 28, no. 3, pp. 3085-3095, 2013.

[19] "Winston Energy Group Limited," [Online]. Available: http://en.winston-battery.com/index.php/products/mobile-power. [Accessed 30 July 2015].

[20] "Department of Energy, Global Energy Storage Database" [Online]. Available: http://www.energystorageexchange.org/projects/153. [Accessed 30 July 2015].

[21] D. Rastler, "Technical Specification for a Transportable Lithium-Ion Energy Storage System for Grid Support Using Commercially Available Lithium-Ion Technology," EPRI, July 2012.

[22] EPRI, "Transportable Energy Storage Systems Project," EPRI, Oct 2009.

[23] "Toshiba," [Online]. Available: https://www.toshiba.co.jp/about/press/2014_01/pr0704.htm. [Accessed 30 July 2015].

[24] Dan Rastler, et. al. "Energy Storage System Costs 2011 update, Executive Summary," EPRI, Feb., 2012.

[25] N. Chen, Z. Qian, I. Nabney and X. Meng, "Wind Power Forecasts Using Gaussian Processes and Numerical Weather Prediction," *IEEE Trans. Power Syst.*, vol. 29, no. 2, pp. 656-665, 2014.

[26] Y. Chakhchoukh, P. Panciatici and L. Mili, "Electric Load Forecasting Based on Statistical Robust Methods," *IEEE Trans. Power Syst.*, vol. 26, no. 3, pp. 982-991, 2011.

[27] D. Saez, F. Avila, D. Olivares, C. Canizares and L. Marin, "Fuzzy Prediction Interval Models for Forecasting Renewable Resources and Loads in Microgrids," *IEEE Trans. Smart Grid*, vol. 6, no. 2, pp. 548-556, 2015.

[28] T. Logenthiran, D. Srinivasan, A. M. Khambadkone and H. N. Aung, "Multiagent System for Real-Time Operation of a Microgrid in Real-Time Digital Simulator," *IEEE Trans. Smart Grid*, vol. 3, no. 2, pp. 925-933, 2012.

[29] P. Kundur, Power System Stability and Control, McGraw-Hill, Inc., 1994.

[30] IEEE Recommended Practice for Sizing Lead-Acid Batteries for Stationary Applications, IEEE, 1997.

[31] A. Yazdani and R. Iravani, *Voltage-Sourced Converters in Power Systems*, Wiley, 2010.

[32] I. Cambridge Systematics, "Traffic Congestion and Reliability (Trends and Advanced Strategies for Congestion Mitigation)," Federal Highway Administration , Sept. 2005.

[33] W. Shi, X. Xie, C. C. Chu and R. Gadh, "Distributed Optimal Energy Management in Microgrids," *IEEE Trans. Smart Grid*, vol. 6, no. 3, pp. 1137-1146, May, 2015.

[34] S. H. Low, "Convex relaxation of optimal power flow—Part II: Exactness," *IEEE Trans. Control Netw. Syst.*, vol. 1, no. 2, pp. 177-189, Jun. 2014.

[35] IESO, "Feed in tariff," [Online]. Available: http://fit.powerauthority.on.ca/. [Accessed 8 Sept. 2015].

[36] P. Poonpun and W. T. Jewell, "Analysis of the Cost per Kilowatt Hour to Store Electricity," *IEEE Trans. Energy Conversion*, vol. 23, no. 2, pp. 529-534, June 2008.

[37] M. Nick, Distrib., R. Cherkaoui and M. Paolone, "Optimal Allocation of Dispersed Energy Storage Systems in Active Distribution Networks for Energy Balance and Grid Support," *IEEE Trans. Power Syst.*, vol. 29, no. 5, pp. 2300 - 2310, Sept. 2014.

[38] "Gurobi Optimization," Gurobi, [Online]. Available: http://www.gurobi.com/. [Accessed 18 Aug 2015].

[39] L. Wang, Model control systems design and implementation Using Matlab, Springer, 2008.

[40] M. AlRashidi and M. El-Hawary, "Hybrid Particle Swarm Optimization Approach for Solving the Discrete OPF Problem Considering the Valve Loading Effects," *IEEE Transactions on Power Systems*, vol. 22, no. 4, pp. 2030-2038, 2007.

[41] Y. M. Atwa, "Distribution System Planning and Reliability Assessment under High DG Penetration," University of Waterloo , Waterloo, Ontario, Canada, 2010.

[42] Hydro One, "Electricity Rates," [Online]. Available: http://www.hydroone.com/MyHome/MyAccount/UnderstandMyBill/Pages/ElectricityRates.aspx. [Accessed 23 Aug. 2015].

[43] IESO, "Power data," [Online]. Available: http://www.ieso.ca/Pages/Power-Data/default.aspx#download.

[44] IESO, "Price schedule," IESO, [Online]. Available: http://fit.powerauthority.on.ca/program-resources/price-schedule. [Accessed 08 Sept. 2015].

[45] M. Nick, R. Cherkaoui and M. Paolone, "Optimal Allocation of Dispersed Energy Storage Systems in Active Distribution Networks for Energy Balance and Grid Support," *IEEE Transactions on Power Systems*, vol. 29, no. 5, pp. 2300-2310, 2014.

[46] S. Schoenung, "Energy Storage Systems Cost Update (A Study for the DOE Energy Storage Systems Program )," SANDIA, Albuquerque, New Mexico, USA, April 2011.

[47] T. G. o. Ontario, "Traveller Information Services 2015," [Online]. Available: http://www.mto.gov.on.ca/english/traveller/trip/traffic_reports.shtml. [Accessed 28 March 2016].

[48] "L.A Traffic," [Online]. Available: http://home.znet.com/schester/calculations/traffic/la/plots/all/index.html. [Accessed 23 Aug. 2015].

[49] H. Abdeltawab and Y.- A-R. I. Mohamed, "Market-Oriented Energy Management of a Hybrid Wind-Battery Energy Storage System Via Model Predictive Control With Constraint Optimizer," *IEEE Trans Indust Electron*, vol. 62, no. 11, pp. 6658 - 6670, Nov. 2015.

[50] J. Eyer, "Electric Utility Transmission and Distribution Upgrade Deferral Benefits from Modular Electricity Storage," Sandia, New Mexico, June 2009.

[51] C. Zhou, K. Qian, M. Allan and W. Zhou, "Modeling of the Cost of EV Battery Wear Due to V2G Application in Power Systems," *IEEE Trans. Energy Convers.*, vol. 26, no. 4, pp. 1041-1050, 2011.

**Hussein Hassan Abdeltawab** was born in Bani-Souwaif, Egypt on April 6, 1987. He received the B.Sc. (with honors), M.Sc. degrees in electrical engineering from Cairo University, Cairo, Egypt in 2009 and 2012, respectively. He is currently working toward the PhD. degree in the Department of Electrical and Computer Engineering, University of Alberta, Edmonton, Canada.

His research interest is in control systems applications in renewable energy systems, energy storage and smart distribution systems.

**Yasser Abdel-Rady I. Mohamed** (M'06, SM'011) was born in Cairo, Egypt, on November 25, 1977. He received the B.Sc. (with honors) and M.Sc. degrees in electrical engineering from Ain Shams University, Cairo, in 2000 and 2004, respectively, and the Ph.D. degree in electrical engineering from the University of Waterloo, Waterloo, ON, Canada, in 2008. He is currently with the Department of Electrical and Computer Engineering, University of Alberta, AB, Canada, as an Associate Professor. His research interests include dynamics and controls of power converters; grid integration of distributed generation and renewable resources; microgrids; modeling, analysis and control of smart grids; and electric machines and motor drives.

Dr. Mohamed is an Associate Editor of the *IEEE Transactions on Industrial Electronics* and *IEEE Transactions on Power Electronics*, and an Editor of the *IEEE Transactions on Power Systems* and *IEEE Transactions on Smart Grid*. Dr. Mohamed is a registered Professional Engineer in the Province of Alberta.